nature microbiology

ARTICLES

https://doi.org/10.1038/s41564-021-00942-8

Entropy-driven translocation of disordered proteins through the Gram-positive bacterial cell wall

David K. Halladin[1,2], Fabian E. Ortega[2], Katharine M. Ng[1,3], Matthew J. Footer[2,4], Nenad S. Mitić[5], Saša N. Malkov[5], Ajay Gopinathan[6], Kerwyn Casey Huang[1,3,7] ✉ and Julie A. Theriot[1,2,4] ✉

In Gram-positive bacteria, a thick cross-linked cell wall separates the membrane from the extracellular space. Some surface-exposed proteins, such as the *Listeria monocytogenes* actin nucleation-promoting factor ActA, remain associated with the bacterial membrane but somehow thread through tens of nanometres of cell wall to expose their amino terminus to the exterior. Here, we report that entropy enables the translocation of disordered transmembrane proteins through the Gram-positive cell wall. We build a physical model, which predicts that the entropic constraint imposed by a thin periplasm is sufficient to drive the translocation of an intrinsically disordered protein such as ActA across a porous barrier similar to a peptidoglycan cell wall. We experimentally validate our model and show that ActA translocation depends on the cell-envelope dimensions and disordered-protein length, and that translocation is reversible. We also show that disordered regions of eukaryotic proteins can translocate Gram-positive cell walls via entropy. We propose that entropic forces are sufficient to drive the translocation of specific proteins to the outer surface.

Surface-exposed proteins are used by commensal and pathogenic bacteria to mediate many processes essential for survival in a mammalian host[1,2]. These host–microbe interactions often involve binding of bacterial proteins to host factors that are too large to diffuse through the nanometre-scale pores of the bacterial cell wall[3]. Surface-exposed proteins must navigate tens of nanometres through the peptidoglycan to reach the outer cell surface to interact with host-encoded partners[4,5]. A further topological challenge is faced by membrane-anchored proteins in Gram-positive bacteria. Mature forms of these proteins span all cellular compartments—starting from the cytoplasm, across the membrane, across a periplasmic-like space[6], and through the nanometre-scale pore-like holes intrinsic to the thick peptidoglycan of all Gram-positive species—to expose their functional surface domains[7,8].

One well-characterized membrane-anchored protein is the virulence factor ActA from the food-borne pathogen *Listeria monocytogenes*[9], which uses bacterial-directed actin-based motility to propel itself through the cytoplasm of a host cell and spread from cell to cell in an infected host[10]. ActA is the only bacterial factor required for host-cell actin assembly[11,12], which it accomplishes through direct interaction with the host-encoded actin-nucleation factor Arp2–Arp3 complex and host-encoded actin-elongation factor VASP in the host cytoplasm[13]. ActA is a large (approximately 600 amino acids) protein with extensive regions of intrinsic disorder[14]. Its Stokes radius (8 nm) is substantially larger than the pores in a Gram-positive cell wall, which limit passive transport to molecules with a radius of <2–3 nm (ref. [3]). As intrinsically disordered proteins can pass through very small pores via reptation[15], it is therefore possible that ActA could thread through cell-wall pores by reptation.

Some form of free energy, often ATP hydrolysis or transmembrane potential[16], is generally required for vectorial transport across membrane barriers that separate cellular compartments. Once a protein exits the cytoplasm, there is no obvious source of chemical free energy to drive directional translocation. How then does ActA translocate its amino (N)-terminal domain while remaining membrane-anchored? Truncation of ActA before the carboxy (C)-terminal transmembrane domain results in secretion of the protein into the extracellular medium[8], suggesting the absence of binding associations between ActA and the cell wall that help or hinder its translocation. In Gram-negative bacteria, chaperones shuttle proteins and other cargo from the inner membrane to the outer membrane[17]. However, no such chaperone-mediated transport mechanism has been described for protein export through the Gram-positive cell wall.

Here we test the hypothesis that confinement of a disordered protein, in this case ActA, in the periplasmic-like space between the membrane and the Gram-positive cell wall results in an entropic force that can drive protein translocation through the cell wall in the absence of chaperones or other machinery.

Results

Biophysical model for ActA translocation across the cell wall. To confirm the distinct topology of ActA as a protein that is both membrane-bound and translocated across the cell wall, we confirmed that most ActA molecules can be extracted from the cell wall in lysogeny broth (LB) and Welshimer's broth (WB; Fig. 1a), and only ActA is extracted from wild-type cells by SDS boiling (Fig. 1b). To determine whether entropy is sufficient to drive ActA

[1]Department of Microbiology and Immunology, Stanford University School of Medicine, Stanford, CA, USA. [2]Department of Biochemistry and Howard Hughes Medical Institute, Stanford University School of Medicine, Stanford, CA, USA. [3]Department of Bioengineering, Stanford University, Stanford, CA, USA. [4]Department of Biology and Howard Hughes Medical Institute, University of Washington, Seattle, WA, USA. [5]Faculty of Mathematics, University of Belgrade, Belgrade, Serbia. [6]Department of Physics, University of California, Merced, CA, USA. [7]Chan Zuckerberg Biohub, San Francisco, CA, USA. ✉e-mail: kchuang@stanford.edu; jtheriot@uw.edu

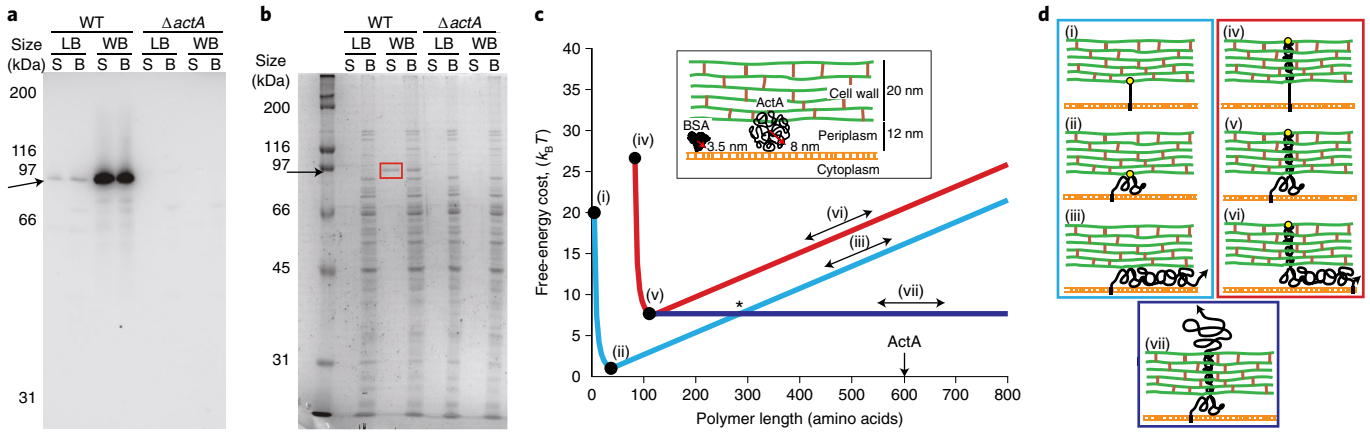

Fig. 1 | Entropy-based model for protein translocation across the Gram-positive cell wall. a, Western blot with anti-ActA of SDS-treated and mechanically disrupted cells through bead-beating demonstrated expression of ActA (arrow) in both LB and WB for the wild type but not the Δ*actA* mutant. In both growth media, comparable amounts of ActA were recovered from SDS-treated and mechanically disrupted cells, indicating that essentially all ActA can be extracted from the cell wall. **b**, Coomassie staining revealed that cytoplasmic proteins are released after mechanical disruption, whereas only ActA (arrow) was extracted by SDS boiling in wild-type cells (red box), indicating its unique translocated topology. S, SDS treated; B, bead-beating; and WT, wild type. **c**, Free-energy cost for a confined self-avoiding polymer, relative to a polymer in solution, plotted as a function of polymer length using a cell-wall thickness of 20 nm, periplasmic thickness of 12 nm, and wall-pore radius of 3 nm (see also Methods and Extended Data Fig. 1). Blue curve, polymer confined to the periplasm; red curve, polymer in which 78 amino acids extend through a pore into the cell wall and all additional amino acids are in the periplasm; and horizontal navy blue line, polymer in an extended state in which 115 amino acids are used to cross the periplasm and cell wall, and all additional amino acids are beyond the outer edge of the cell wall. The asterisk marks the critical length beyond which it is energetically favourable for the polymer to extend through the cell wall. Insert: schematic of the cell surface that includes the relative sizes of ActA and bovine serum albumin (PDB ID 1E7I), which have similar molecular weights but very different Stokes radii. **d**, Schematic depicting polymer topology in different states. States (i)–(iii) (blue box) correspond to the blue curve in **c**, states (iv)–(vi) (red box) correspond to the red curve in **c** and state (vii) (fully translocated) corresponds to the navy blue curve in **c**. The gold circles signify constraints where one point in the polymer is fixed to either the inner surface of the cell wall (states (i) and (ii)) or the outer surface (states (iv) and (v)). The arrows denote the topologies of variable polymer length (states (iii), (vi) and (vii)) and correspond to the portions of the curves in **c** labelled with double-headed arrows.

translocation, we developed a physical model for the confinement of a disordered polymer in the periplasm and cell wall (Methods), with three parameters characterizing the cell-envelope dimensions: wall thickness, periplasmic thickness and wall-pore radius. We treat the polymer as a self-avoiding chain with a persistence length estimated from ActA Stokes radius measurements[14]. Our model predicts that, due to the free-energy cost of crossing the wall, short polymers will remain in the periplasm even with lengths at which they experience some confinement, because partial confinement within a narrow cell-wall pore adds substantially to the entropic penalty. However, there is a critical length beyond which the entropic cost of periplasmic confinement can be relieved by extending through the wall to access the unconfined exterior (Fig. 1c,d and Methods). The length of ActA is greater than the predicted critical length for a wide range of plausible parameter values (Extended Data Fig. 1). Thus, in theory, entropy alone should be sufficient to drive the translocation of an ActA-like polymer through a porous barrier such as the Gram-positive cell wall, resulting in a final configuration in which the C terminus remains anchored to the membrane and the N-terminal domain can interact with host-cell binding partners.

Truncation of ActA shows that translocation is reversible. Our model implicitly assumes that the transition between an extended and periplasmic state is reversible, whereby the polymer topology would re-equilibrate if the polymer length were altered after translocation (Fig. 2a). For a large range of parameters (Extended Data Fig. 1), our entropic model predicts a sigmoidal transition for the majority fraction of ActA molecules, from fully extended to retained within the periplasm (Fig. 2a). To determine whether truncation of full-length ActA below a critical length results in re-equilibration to a periplasmic state (Fig. 2b), we engineered ActA constructs with an internal TEV protease recognition site at various locations (Fig. 2c). To detect ActA translocation, we used an antibody raised against the VASP-binding domain of ActA, which is normally exposed on the external surface of the bacterial cell wall[13]. All constructs were designed with the protease-cleavage site N-terminal of this epitope so that the epitope would remain anchored to the bacterial membrane following protease cleavage. All constructs displayed comparable cleavage efficiency after TEV treatment, and cleaved ActA molecules showed no apparent differences in stability (Fig. 2d). Because antibodies are too large to diffuse through wall pores[3], we used immunofluorescence microscopy to differentiate between ActA molecules that extended through the wall and those confined to the periplasm. The removal of ≥166 amino acids resulted in a significant decrease in antibody labelling, whereas shorter truncations had little effect (Fig. 2e and Extended Data Fig. 2); these data confirm that translocation is reversible. We also constructed genetic truncations of 100 or 200 amino acids from the N terminus of ActA (Extended Data Fig. 3). Consistent with our TEV data, the 100-amino-acid truncation exhibited similar antibody labelling to full-length ActA, whereas labelling of the 200-amino acid truncation decreased significantly (Fig. 2f) to a level comparable to our TEV-166 construct. Thus, truncation of ActA past a critical length decreases the fraction of molecules extending through the wall.

Cell-wall thickness is inversely correlated with ActA translocation efficacy. To determine whether differences in envelope architecture affect the length dependence of polymer translocation, we decreased wall thickness by deleting the *wall* gene (Fig. 3a,b), which encodes a regulator of the WalRK two-component system that coordinates wall synthesis with growth[18,19]. We observed similar antibody labelling on expression of full-length ActA or its genetic

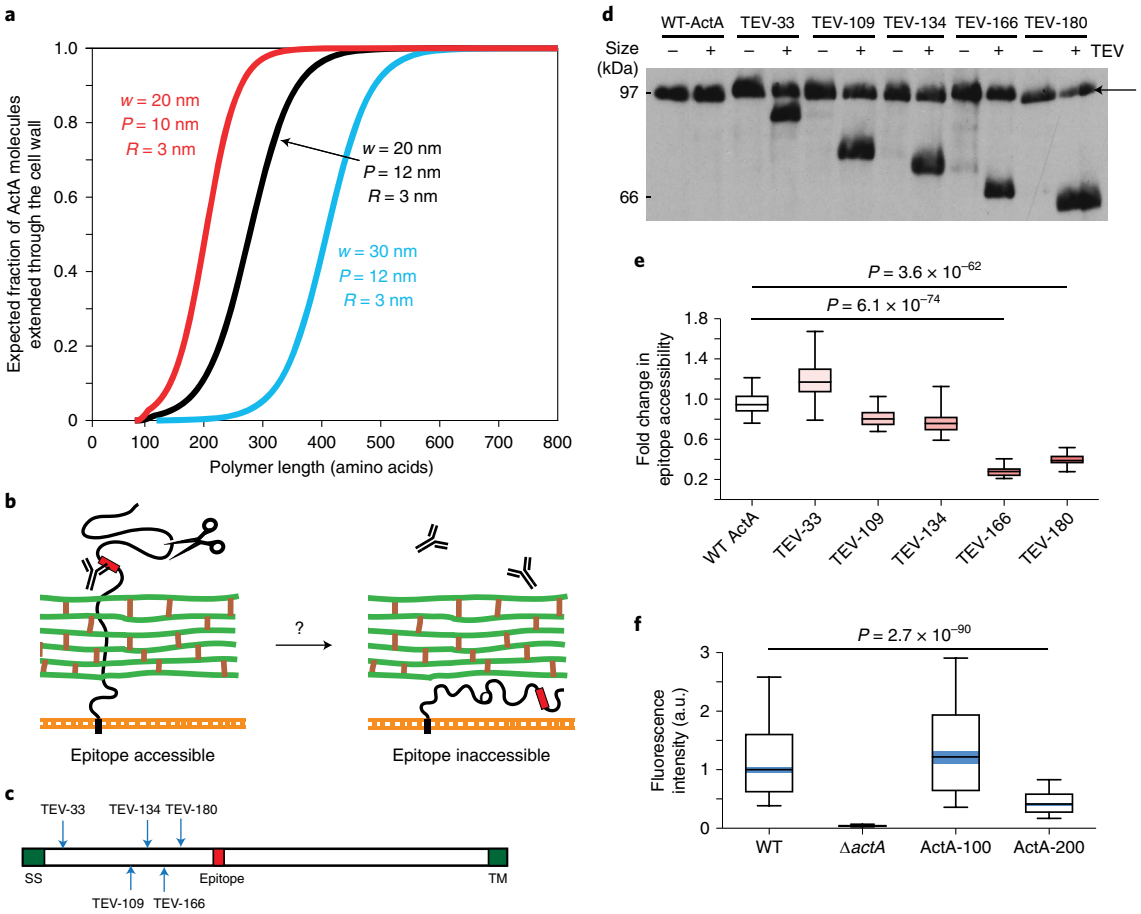

Fig. 2 | Length of ActA and retention in the periplasm. a, Expected fraction of ActA molecules in an extended state as a function of polymer length (Methods) for various cell-wall-thickness (*w*), periplasmic-thickness (*P*) and wall-pore-radius (*R*) values. **b**, Following cleavage by the TEV protease, an ActA molecule can remain extended (left) or transition to a periplasmic state (right). **c**, Schematic of ActA showing the position of the signal sequence (SS), transmembrane domain (TM), TEV-cleavage sites (arrows), and antibody recognition site. **d**, Western blot with an antibody against the proline-rich repeat region of ActA (anti-ActA-PRR) for strains carrying each construct before (−) and after (+) treatment with TEV protease. The arrow indicates full-length ActA. **e**, The fold change in immunofluorescence intensity corresponding to epitope accessibility with anti-ActA-PRR comparing untreated and TEV protease-treated populations was significant only for the TEV-166 and TEV-180 constructs (cleavage of 166 and 180 amino acids, respectively). From left to right: untreated, $n = 515$, 541, 382, 508, 277, and 505 cells; TEV-treated, $n = 384$, 472, 452, 488, 667, and 625 cells. **f**, Truncation of 200 (ActA-200), but not 100 (ActA-100), amino acids from the C terminus of ActA resulted in significantly reduced immunofluorescence intensity. Essentially no labelling was detected in the Δ*actA* mutant. The blue shading indicates the confidence intervals for the median. **e**,**f**, The fluorescence intensities were normalized so that the median of the wild-type *L. monocytogenes* strain was 1. The box shows 25th and 75th percentiles with the median as a horizontal line, and whiskers are 10th and 90th percentiles. WT, wild-type; and a.u., arbitrary units.

truncations (Fig. 3c), indicating that, unlike in wild-type cells (Fig. 2f), the 200-amino-acid truncation was able to translocate. The cell wall became thicker during growth in WB broth (Fig. 3a,b), which should impose a larger barrier, increasing the critical length for entropic translocation. Labelling of full-length ActA was now significantly higher than both truncations (Fig. 3d), indicating that the 100-amino-acid truncation was compromised in translocation across the thicker wall, consistent with the predicted increase in critical length.

Only a longer form of ActA can traverse the thicker *Bacillus subtilis* cell wall. Next, we expressed ActA in a *B. subtilis* strain lacking the major proteases[20], motivated by previous studies showing that *B. subtilis* has a thicker cell wall and periplasmic space than *L. monocytogenes*[6,21]. Consistent with our model predictions, we observed no antibody labelling when full-length ActA was expressed (Fig. 4a). Digestion of the wall using lysozyme[19] resulted in ActA labelling (Fig. 4b), indicating that the protein was expressed, secreted, and anchored at the membrane but was unable to translocate through the *B. subtilis* wall. To determine whether a longer disordered protein could translocate in *B. subtilis*, we expressed the iActA (1,080 amino acids) protein from *Listeria ivanovii*. Much like ActA, iActA is a transmembrane protein that promotes actin polymerization at the surface[22,23] and is predicted to have an almost entirely disordered N-terminal domain (Fig. 4c). We observed labelling of iActA on the *B. subtilis* surface (Fig. 4d), suggesting that iActA experiences enough confinement in the periplasm to overcome the entropic barrier and navigate across the wall.

Disordered nuclear pore-complex proteins can translocate through the cell wall. One prediction of our model is that any sufficiently long disordered protein should translocate through a Gram-positive cell wall provided there is sufficient periplasmic confinement. To test this prediction, we used disordered regions from nuclear pore-complex proteins with similar lengths and Stokes radii to ActA[24]. To direct these eukaryotic protein regions to the

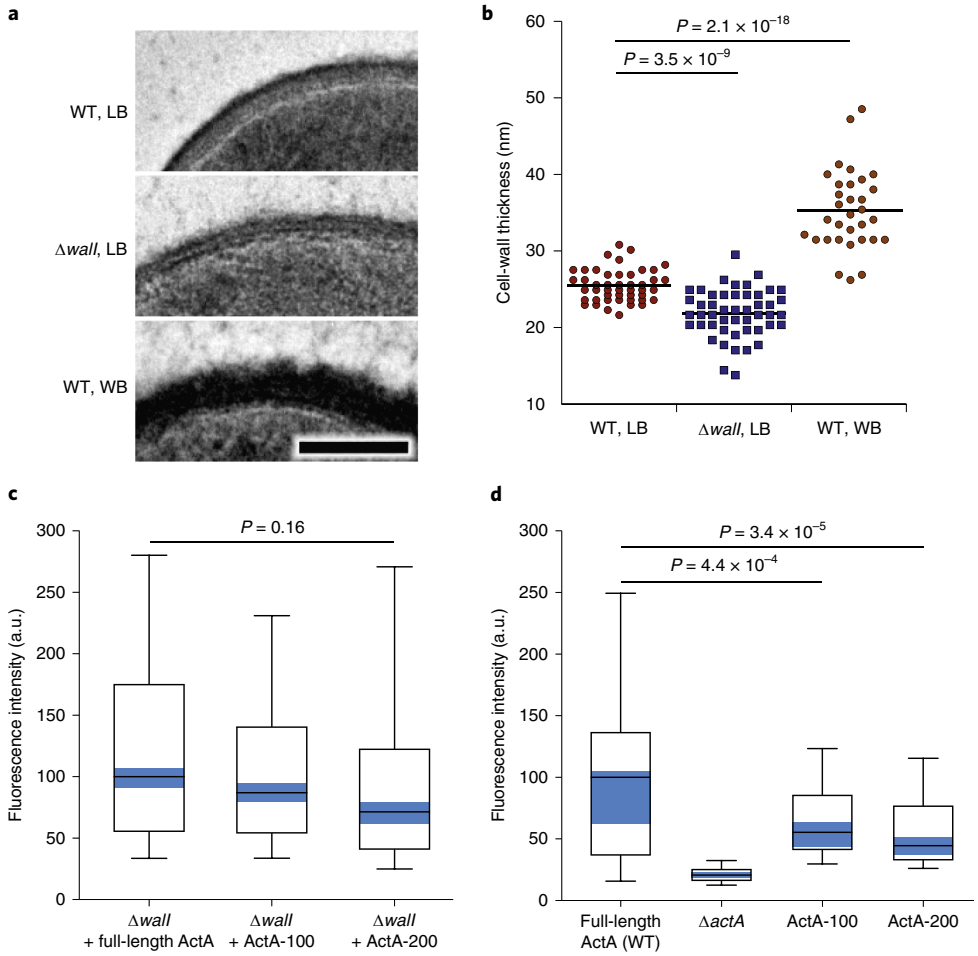

Fig. 3 | Cell-wall thickness and ActA translocation. a, Electron micrographs of wild-type *L. monocytogenes* cells in LB medium (top), cells with a *wall* deletion in LB medium (middle), and wild-type cells in WB medium (bottom). Scale bar, 100 nm. **b**, Deletion of *wall* decreased wall thickness relative to wild type and growth in WB increased wall thickness relative to growth in LB medium. **c**, The thinner cell wall of Δ*wall* cells allowed translocation even after truncation of 200 amino acids at the C terminus of ActA. Immunofluorescence intensities from labelling with anti-ActA-PRR were normalized so that the median of the wild-type strain was 1. **d**, In WB medium, labelling was significantly lower in both truncation mutants compared with wild-type cells expressing full-length ActA. Fluorescence intensities were normalized so that the median of the wild-type strain was 1. **c**,**d**, Boxes show the 25th and 75th percentiles with the median as a horizontal line, and whiskers indicate the 10th and 90th percentiles. The blue shading indicates confidence intervals for the median. WT, wild type; a.u., arbitrary units.

L. monocytogenes surface, we created chimaeric proteins, using the signal sequence and transmembrane domain from ActA, that were stably produced in *L. monocytogenes* (Extended Data Fig. 4a). Remarkably, the disordered regions from Nsp1 and Nup1 translocated and adopted a polar distribution similar to ActA localization (Fig. 5a,b and Extended Data Figs. 4b,c, 5) over several generations (Extended Data Fig. 5). Removal of the transmembrane domain from the Nsp1 construct resulted in secretion into the extracellular medium and an absence of immunofluorescence signal at the cell surface (Extended Data Fig. 4d), demonstrating that labelling required anchoring to the membrane and not non-specific binding to the wall.

To further test the generality of our model, we expressed Nsp1 in *Staphylococcus aureus*, a round bacterium with a cell-wall thickness comparable to that of *L. monocytogenes* and a thinner periplasm than *B. subtilis*[25]. The N-terminal signal sequence of protein A and C-terminal transmembrane domain of ActA were used for Nsp1 secretion and membrane anchoring, respectively. Antibody-accessible Nsp1 stably presented across the *S. aureus* surface (Fig. 5c), similar to native protein A[26,27]. Thus, exogenous disordered proteins, even those of eukaryotic origin, can translocate through the cell wall of *L. monocytogenes*, *B. subtilis*, and *S. aureus*. We applied bioinformatics to identify long disordered regions in surface proteins of many Gram-positive species, including the *S. aureus* membrane-anchored surface protein EbpS that extends through the wall to bind host elastin[30], suggesting that entropy-driven translocation may be widespread (Fig. 6 and Table 1).

ActA translocation is unlikely to require an active process. Although our model predicts that entropy can be sufficient for translocation, we considered the possibility that an active process is also required. For example, the *cis-trans*-prolyl-isomerase PrsA2 could in principle contribute to translocation as ActA contains several proline-rich domains. *L. monocytogenes* Δ*prsA2* cells are defective in the secretion of many proteins[28], including listeriolysin O (Extended Data Fig. 6a); ActA expression did decrease relative to the wild-type in *prsA2* transposon-insertion mutants but the same amount of expressed protein was extracted by both SDS and mechanical disruption, indicating extension beyond the wall (Extended Data Fig. 6b). Antibody labelling confirmed the translocation of ActA in the *prsA2* mutant (Extended Data Fig. 6c). Moreover, the proline-rich domains of ActA bound the relevant

Table 1 | Surface proteins with a predicted disordered region of at least 250 amino acids for *L. monocytogenes*, *S. aureus*, *Lactobacillus acidophilus*, *Enterococcus faecalis*, *Streptococcus pyogenes*, *Bacillus anthracis*, and *Lactococcus lactis*

Species	Gene	Function	Disordered region length (amino acids)
L. monocytogenes	*actA*	Actin-assembly-inducing protein	579
	lmo1105	Hypothetical protein	273
	lmo1799	Peptidoglycan-binding protein	473
	lmo2287	Phage tape-measure protein	283
S. aureus	*spa*	IgG-binding protein A	368
	coa	Staphylocoagulase	438
	geh	Glycerol-ester hydrolase	265
	sdrC	Ser-Asp-rich fibrinogen-binding, bone sialoprotein-binding protein	285
	sdrD	Ser-Asp-rich fibrinogen-binding, bone sialoprotein-binding protein	336
	clfA	Fibrinogen-binding protein A, clumping factor	461
	SA0743	Hypothetical protein, similar to staphylocoagulase	295
	htrA	Serine protease	392
	ebhA	Hypothetical protein, similar to streptococcal adhesin Emb	383, 517, 260, 457, 1,009, 739, 369, 821, and 429
	ebhB	Hypothetical protein, similar to streptococcal adhesin Emb	921
	ebpS	Elastin-binding protein	316
	SA1559	Hypothetical protein, similar to caldesmon	398
	SA1577	Hypothetical protein, similar to FmtB	301
	fmtB	FmtB protein	948 and 418
	fnbB	Fibronectin-binding protein	468
	fnb	Fibronectin-binding protein	469
	clfB	Clumping factor B	324
	SA2439	Hypothetical protein	386
	SA2447	Hypothetical protein, serine-rich adhesin for platelets	1,673
	lip	Triacylglycerol lipase	265
L. acidophilus	*LBA1020*	Mucus-binding protein	256
	LBA1019	Mucus-binding protein	260
	fmtB	Surface protein	1,251 and 1,098
	LBA1637	Membrane protein	461
	LBA1633	Surface protein	591
	LBA1634	Surface protein	376
E. faecalis	*EF0093*	Cell wall surface anchor family	359
	EF0146	Surface exclusion protein	349 and 341
	EF0502	Hypothetical protein	314
	EF1099	Collagen adhesin protein	344
	EF1523	Hypothetical protein	316
	EF1877	Hypothetical protein	283
	EF2318	M24/M37 family peptidase	327
	EF3023	Polysaccharide lyase family	338
	EF3173	Hypothetical protein	308
	EF3314	Cell wall surface anchor family	289
S. pyogenes	*spyM18_0256*	Surface exclusion protein	266
	spa	Protective antigen	394
	emm18	M18 protein	339
B. anthracis	*BAS0454*	Phage tape-measure protein	371
	BAS1009	Hypothetical protein	316

Continued

Table 1 | Surface proteins with a predicted disordered region of at least 250 amino acids for *L. monocytogenes*, *S. aureus*, *Lactobacillus acidophilus*, *Enterococcus faecalis*, *Streptococcus pyogenes*, *Bacillus anthracis*, and *Lactococcus lactis* (continued)

Species	Gene	Function	Disordered region length (amino acids)
	BAS3021	Cell wall anchor domain protein	331
	BAS4630	Spore germination protein	283
L. lactis	*lcnD*	Lactococcin A ABC transporter permease	260
	yihD	Hypothetical protein	459
	yjaE	Hypothetical protein	276
	yoiC	Hypothetical protein	509
	yqfG	Hypothetical protein	767
	usp45	Hypothetical protein	316

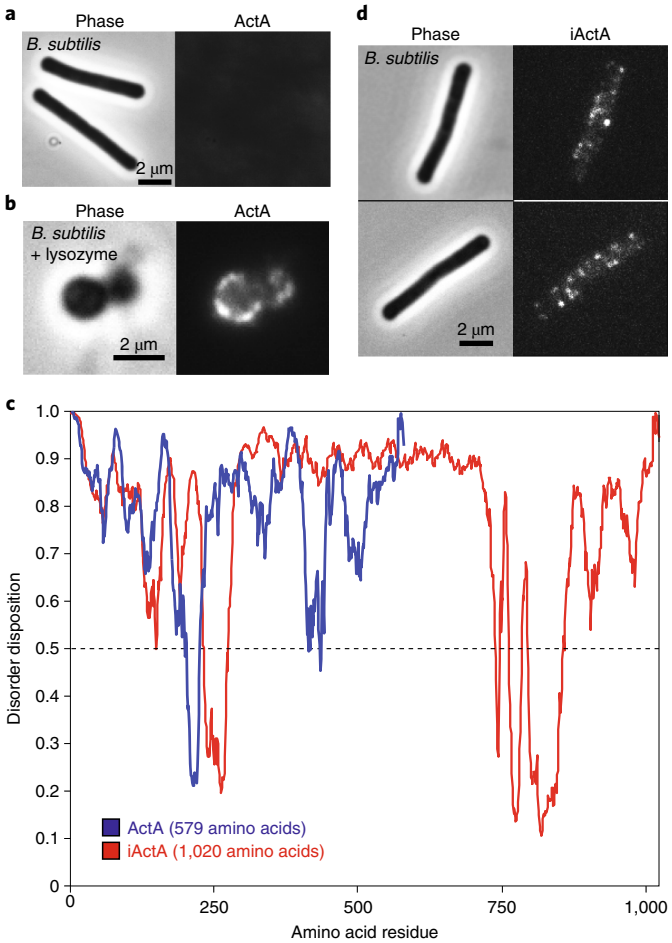

Fig. 4 | The disordered transmembrane protein iActA extends through the *B. subtilis* cell wall. a, *B. subtilis* cells expressing the 65-kDa ActA protein exhibited no appreciable immunofluorescence labelling with anti-ActA, indicating minimal translocation (right). **b**, Labelling of lysozyme-treated *B. subtilis* expressing ActA with anti-ActA showed ActA associated with the membrane of the spheroplast. **c**, Disorder prediction results for the extracellular regions of ActA and iActA using the PONDR-FIT predictor. **d**, Punctate immunofluorescence labelling with anti-ActA was observed in *B. subtilis* engineered to express the 108-kDa iActA protein, suggesting that a longer disordered protein was able to translocate across the relatively thick *B. subtilis* cell wall compared with that of *L. monocytogenes*. **a**,**b**,**d**, Phase-contrast images are shown on the left.

domain of VASP in the *prsA2* mutant (Extended Data Fig. 6d), and the *prsA2*-mutant bacteria formed normal actin-rich comet tails in infected host cells (Extended Data Fig. 6e). Thus, PrsA2 is not required for ActA translocation or its normal function. We hypothesized that any other active translocation would most probably result from mechanical coupling of wall translocation to secretion through the membrane, driven by the ATPase SecA or the ribosome[16,29]. The force from secretion could possibly push a membrane-anchored protein through the wall if the transmembrane anchor were located at the C terminus (as in native ActA); however, such a mechanism would not be possible for proteins with an N-terminal transmembrane domain, as both ends would remain membrane-associated until secretion was complete (Fig. 5d). To test whether mechanical work by the secretion apparatus is required for translocation, we anchored Nsp1 to the membrane using the N-terminal transmembrane domain from *L. monocytogenes* penicillin-binding proteins. We observed translocation of both Nsp1 constructs (Fig. 5e,f), indicating that translocation can occur after secretion has completed, with the final protein orientation opposite to that of our previous experiments (C terminus out versus N terminus out). Constructs containing Nsp1 flanked by both N- and C-terminal transmembrane domains remained entirely confined to the periplasmic space (Extended Data Fig. 4e).

Discussion

Our results show that entropy-driven translocation of disordered proteins through a Gram-positive cell wall depends on both the cell-surface geometry and the length of the translocating protein but does not require any particular sequence or polypeptide orientation.

Although we focused our study on the translocation of disordered membrane-anchored proteins, any sufficiently long disordered regions may promote translocation of secreted and wall-associated proteins through the cell wall. The development of methods to study translocation dynamics would complement the steady-state approaches we report here.

In conclusion, unlike outer-membrane biogenesis in Gram-negative bacteria, which requires chaperones[17] and is sometimes coupled to the hydrolysis of intracellular ATP[31], entropy-driven translocation of disordered proteins across the Gram-positive cell wall seems to occur independently of specific machinery or any energy input.

Methods

Biophysical model. Previous theoretical work has investigated polymer translocation through a porous entropic barrier[34–41]. Here we present a model for the translocation of an intrinsically disordered protein through the Gram-positive cell wall, with the goal of making qualitative predictions for how the critical length should scale with the key variables of the cell-wall pore size (R), periplasmic

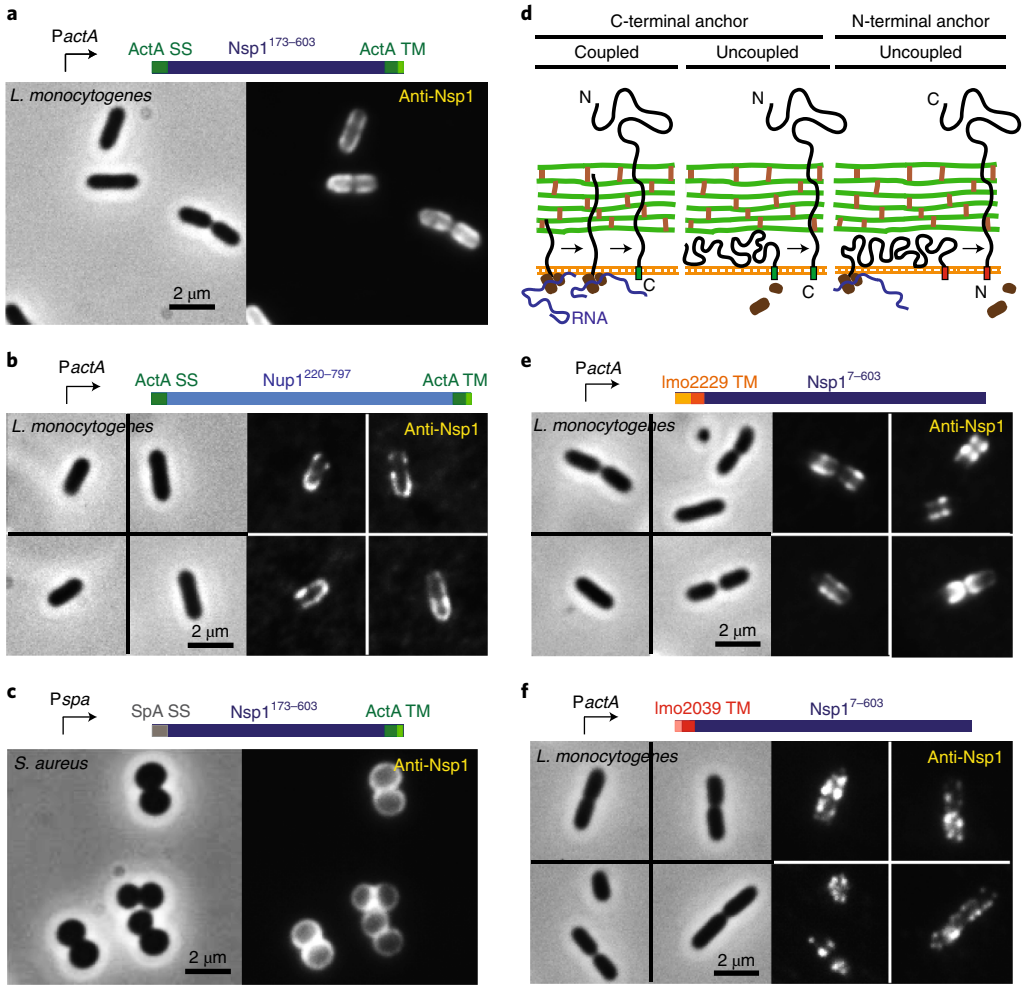

Fig. 5 | Disordered nuclear pore proteins traverse the bacterial cell wall. a–**c**,**e**,**f**, Schematics of protein constructs indicating the promoter (P*actA* or P*spa*), the signal sequence (ActA, Spa, Imo2229, or Imo2039), the protein coding region (Nsp1 or Nup1) and the presence or absence of a C-terminal anchor domain are shown above each set of images, with phase-contrast images on the left and immunofluorescence images on the right. **a**,**b**, Immunofluorescence showing surface presentation and polarized localization of Nsp1 (**a**) and Nup1 (**b**) in *L. monocytogenes* when expressed with the promoter, signal sequence, and C-terminal anchor from ActA. **c**, Surface presentation of Nsp1 in *S. aureus*, expressed with the promoter and signal sequence from protein A (SpA). **a**–**c**, SS, signal sequence; TM, transmembrane domain. **d**, Schematic of possible polymer topologies during secretion through the membrane. Secretion and translocation can be either coupled or uncoupled in proteins with a C-terminal anchor (left), whereas these processes would need to be uncoupled for proteins anchored at the N terminus (right). **e**, Surface presentation of Nsp1 with an N-terminal transmembrane domain from the penicillin-binding protein Imo2229. Note the predominant localization to the mid-cell region. **f**, Surface presentation and punctate lateral-wall localization of Nsp1 with an N-terminal transmembrane domain from Imo2039.

thickness (P), and cell-wall thickness (w); the critical length will depend on these variables (Extended Data Fig. 1) but the qualitative conclusions of our study are general features of the model.

Cell-surface properties. The bacterial cell surface was modelled using three parameters: w, P, and R. To estimate w, we used previous measurements from conventional and cryogenic transmission electron microscopy (TEM)[6,21,25,42,43] as well as our own measurements (Fig. 3b). Cryogenic TEM measurements were used to approximate the value for P[6,21,25]; a distinct periplasmic space in *L. monocytogenes* has not been observed using conventional TEM, possibly because of poor preservation of the structure during fixation, dehydration, and/or embedding. For R, we modelled a continuous pore through the cell wall. Although a continuous pore has not been observed, the cross-linked nature of the sacculus creates an inherently porous structure and the quantitative predictions of our model do not depend on the precise geometry of the pore. Isolated sacculi of *Escherichia coli* and *B. subtilis* have a mean pore radius of approximately 2–3 nm, measured by the permeation of fluorescent dextrans[3], suggesting that a typical R that may be a molecular property of peptidoglycan and hence reasonably conserved across bacterial species.

Kuhn length of ActA. The extracellular region of ActA has no apparent secondary structure and a Stokes radius (R_H) of approximately 8 nm (ref. [14]). Because of the lack of secondary structure, we used a simple polymer physics model to describe the behaviour of ActA[44]. For a self-avoiding polymer, the radius of gyration (R_G) can be estimated as $1.58R_H$ (ref. [45]). The estimated persistence length (l_p) of such a polymer is

$$l_p = \frac{\left(\sqrt{6}R_G\right)^{1/(1-\nu)}}{2L^{\nu/(1-\nu)}}$$

where L is the length of the completely stretched protein and ν is the Flory exponent. For a freely jointed chain, $\nu = 0.5$ and $l_p = \frac{3R_G^2}{L}$, but for more realistic scenarios, $\nu > 0.5$ (ref. [46]). For the plots in Figs. 1,2 and Extended Data Fig. 1, we modelled ActA as a self-avoiding polymer with $\nu = 0.59$ (ref. [40]); the qualitative predictions of our model are insensitive to the choice of ν. For a protein of 600 amino acids, the completely stretched length would be approximately 228 nm, assuming each amino acid occupies 0.38 nm. Thus, the l_p of ActA is 0.875 nm, giving an effective Kuhn length (a) $= 2l_p \approx 1.75$ nm or 4.61 amino acids. Hereafter, we refer to all lengths in units of a.

Blob approximation. A polymer subject to confinement or tension has a distribution of conformations whose statistical properties can be approximated as those of a connected series of 'blobs', wherein each blob represents the maximum

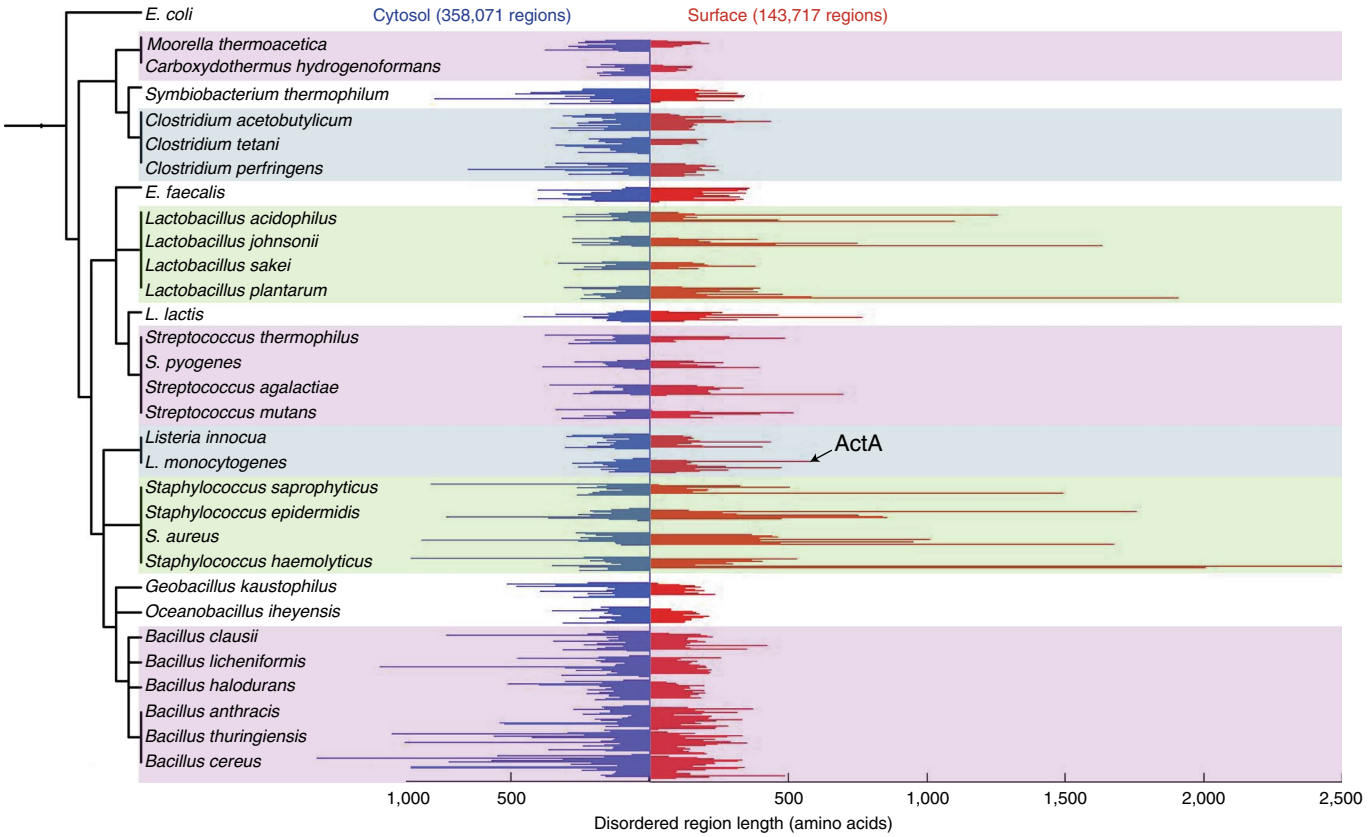

Fig. 6 | Disordered regions are common in surface proteins of Gram-positive bacteria. To determine whether entropy-driven translocation is widespread among Gram-positive bacteria, we analysed 30 bacterial proteomes for surface proteins with long disordered regions. Surface proteins (disordered regions denoted as red bars) were identified based on the presence of a predicted transmembrane domain, signal sequence, or LPXTG motif. Proteins that were not predicted to be surface proteins were considered cytosolic (disordered regions denoted as blue bars). Disordered regions were determined using the disorder predictor VSL2B[32,33]. The shaded regions highlight groups of phylogenetically related bacteria. We found long disordered regions in surface proteins in most Gram-positive species, including disordered regions longer than 500 amino acids in *Listeria monocytogenes* and *Lactococcus lactis*, and *Lactobacillus*, *Streptococcus* and *Staphylococcus* species. Consistent with our model, the *S. aureus* membrane-anchored surface protein EbpS, which extends through the cell wall to bind host elastin[30], was predicted to have an entirely disordered ectopic domain. In some Gram-positive bacteria, there is a surface structure external to the cell wall, such as an S-layer or mycolate layer, that might negate the entropic benefit of translocation by creating a confined environment beyond the cell wall. For many of the bacterial species that have an S-layer, such as *Clostridium* species and *E. faecalis*, we identified few surface proteins with long disordered regions, suggesting that the need for translocation might drive the evolution of long disordered regions and that entropic translocation is less prevalent or not utilized by these species. See also Table 1.

size of a segment of the polymer below which the confinement and tension effects can be ignored[40]. Scaling then argues that the number of subunits in each blob of size r is $g \propto r^{1/\nu}$ (assuming $g \gg 1$ or $r > l_p$, which is the case for the typical confinements and extensions we consider).

Entropic cost of confinement. To estimate the entropy of a polymer confined within a periplasm of thickness $P = 2p$, we assume that $n_p \gg p$, where n_p is the number of Kuhn lengths of the polymer situated in the periplasm. The number of effective blobs in the periplasm is $N_b = n_p/g$, with $g \sim p^{1/\nu}$. The entropic cost (F) of polymer confinement in the periplasm scales as k_BT per blob[40], where k_B is the Boltzmann constant and T is temperature, giving

$$F_p^c = k_B T n_p / p^{1/\nu}. \quad (1)$$

Using a similar argument[40], the entropic cost of confinement of a polymer in a pore of radius R in the cell wall scales as $1/R^{1/\nu}$.

Entropic cost of stretching. A polymer will also incur an entropic cost if it is stretched beyond its preferred, unperturbed size. If a polymer of unperturbed radius less than p is stretched across the periplasm, it can be regarded as a chain of blobs of radius r. Each blob will have g subunits, where $g \sim r^{1/\nu}$ and the number of blobs needed to cross the periplasm is p/r. Thus, the total number of subunits in the periplasm is

$$n_p = p/r \times g = p r^{1/\nu - 1},$$

which results in the relation $r = (n_p/p)^{\nu/(1-\nu)}$. Thus, the stretching free-energy cost is[40]

$$F_p^s = k_B T p/r = k_B T p^{1/(1-\nu)} / n_p^{\nu/(1-\nu)}. \quad (2)$$

A similar argument can be made for stretching across the cell wall, replacing p with w.

Free-energy cost. To determine the free-energy landscape, we calculated the free-energy cost of each configuration of the polymer relative to a polymer of the same length in an unconfined solution as a function of p, w, R, and n. Using equations 1 and 2, the free-energy costs in the periplasm and cell wall are

$$F_p^s = k_B T p^{1/(1-\nu)} / n_p^{\nu/(1-\nu)} \quad \text{for } n_p < n_p^c = p^{1/\nu}$$

$$F_p^c = k_B T n_p / p^{1/\nu} \quad \text{for } n_p > p^{1/\nu}$$

and

$$F_w^s = k_B T w^{1/(1-\nu)} / n_w^{\nu/(1-\nu)} \quad \text{for } n_w < n_w^c = wR^{(1-\nu)/\nu}$$

$$F_w^c = k_B T n_w / R^{1/\nu} \quad \text{for } n_w = wR^{(1-\nu)/\nu}$$

respectively. We do not consider $n_w > wR^{(1-\nu)/\nu}$ (at which point the blobs are of size R) as any additional polymer subunits can be moved to the unconfined exterior

or the periplasm where there is less confinement and therefore results in lower free energy.

Critical length. To calculate the critical length for polymer translocation, we determined the minimum free-energy cost E_{cross} for crossing the periplasm and cell wall and compared this value with the total free-energy cost for the entire polymer to be confined to the periplasm. Translocation through the cell wall becomes favourable when the free-energy cost of periplasmic confinement E_{peri} is greater than E_{cross}, although there is an energy barrier for cell-wall crossing. The condition that determines the critical length n_c is when $E_{peri}=E_{cross}$:

$$k_B T n_c/p^{1/\nu} = k_B T(n_p^c/p^{1/\nu} + n_w^c/R^{1/\nu}).$$

The critical length is then given by

$$n_c = p^{\frac{1}{\nu}}\left(1+\frac{w}{R}\right).$$

Fraction of molecules extending through the cell wall. The expected fraction of molecules in an extended state at equilibrium is

$$\frac{e^{-\varepsilon_E/k_B T}}{e^{-\varepsilon_E/k_B T}+e^{-\varepsilon_P/k_B T}} = \frac{e^{\Delta\varepsilon/k_B T}}{1+e^{\Delta\varepsilon/k_B T}}$$

where ε_E and ε_P are the free-energy costs for a polymer in an extended state and periplasmic state, respectively, and $\Delta\varepsilon=\varepsilon_P-\varepsilon_E$.

Strains and growth conditions. Unless otherwise noted, all strains were cultured at 37 °C with aeration.

L. monocytogenes. TEV-cleavage experiments were performed using a PrfA* strain of *L. monocytogenes* that constitutively expresses ActA[47]. These strains were cultured for 12–16 h in 1.5X LB medium containing 7.5 μg ml^{-1} chloramphenicol (Cm; Sigma) until reaching an optical density at 600 nm (OD_{600}) = 0.4–0.5. All other experiments were performed in the 10403S background. Expression of *actA* (10403S strains) from the native promoter[7] or an isopropyl-β-D-thiogalactoside (IPTG)-inducible promoter[48] was induced as previously described. Bacteria were cultured overnight in BHI medium containing 7.5 μg ml^{-1} Cm and the overnight cultures were then spun down and resuspended in the appropriate medium. To express ActA from the SPAC/lacOid promoter, the cultures were diluted 1:50 into BHI medium containing 7.5 μg ml^{-1} Cm and 0.5 mM IPTG. To express ActA from its native promoter, the cultures were diluted 1:25 into an induction medium of LB supplemented with 25 mM α-D-glucose 1-phosphate (Sigma) and approximately 1–2% (wt/vol) activated carbon pellets[49,50].

B. subtilis. Strain WB600 (ref. [20]) was cultured overnight in LB medium containing 5 μg ml^{-1} Cm and then diluted 1:25 in LB medium containing 5 μg ml^{-1} Cm and cultured until early-log phase was reached (OD_{600} = 0.2–0.25). The cultures were then spun down and resuspended in an equal volume of LB medium containing 5 μg ml^{-1} Cm (pH 6.0) and cultured for 2 h. ActA and iActA were expressed from the *gsiB* promoter, which is induced during acid stress[51,52].

S. aureus. Strain RN6390 (Δ*spA*) was cultured overnight in TSB medium containing 5 μg ml^{-1} Cm and then diluted 1:50 in TSB medium containing 5 μg ml^{-1} Cm and cultured until mid-log phase was reached (OD_{600} = 0.5–0.7). For *S. aureus*, Nsp1 expression was driven by the *spA* promoter.

Strain construction. For *L. monocytogenes* constructs, the site-specific bacteriophage integration vectors pPL1 and pPL2 were used as previously described[53]. For ActA constructs with an internal TEV recognition site, pPL1 was used, whereas pPL2 was used for nuclear pore-complex protein constructs. For IPTG-inducible expression of ActA, we used the previously described *L. monocytogenes* expression vector pHLIV2 (ref. [48]), which is an integration vector derived from pPL2 (strain created by M. Rengarajan, Theriot laboratory). For expression of ActA and iActA in *B. subtilis*, we used the previously described expression vector pHCMC03 (ref. [52]). We used the shuttle vector pOS1 (ref. [54]) for Nsp1 expression in *S. aureus*. Disruption of *walI* in the ActA truncation mutants was performed by U153 phage transduction of a *walI::Tn* mutant (obtained from the Portnoy laboratory) into the appropriate truncation mutant strain.

Overlap extension PCR was used to insert the TEV protease recognition site into ActA. The DNA sequence of the TEV recognition site was used as the overlapping region. The desired sequences, as specified in the 'Additional strain information' section, were amplified from genomic preparations of the *L. monocytogenes* strain 10403S (ActA, lmo2229 and lmo2039), *L. ivanovii* strain ATCC19119 (iActA), *Saccharomyces cerevisiae* strain S288C (Nsp1 and Nup1), or *S. aureus* strain RN4220 (SpA).

Slide preparation. Coverslips (18 mm; no. 1.5) were cleaned in concentrated HCl for 4 h, followed by extensive washing with ddH_2O. The coverslips were then rinsed in 95% ethanol, followed by 100% ethanol before being transferred to a glass Petri dish and autoclaved.

Immunofluorescence. Unless otherwise noted, bacteria were fixed using formaldehyde at a final concentration of 3.7%. The fixed bacterial culture (60 μl) was placed on an acid-washed coverslip and incubated at room temperature for 10–30 min, depending on the culture density. The coverslips were washed twice with PBS and then incubated with primary antibody at the appropriate dilution for 1 h. Antibodies were used at the following dilutions: rabbit polyclonal anti-peptide antibody against the first proline-rich repeat of ActA (anti-ActA-PRR), 1:500; rabbit polyclonal antibody against full-length ActA (anti-ActA), 1:2,000; and rabbit polyclonal antibody against the FG-region of Nsp1 (anti-Nsp1; gift from M. Rexach, University of California at Santa Cruz), 1:2,000. The coverslips were washed twice with PBS and then incubated with Alexa Fluor-488 goat anti-rabbit (Invitrogen) at 1:1,000 for 1 h. The coverslips were washed three times with PBS, blotted to remove excess liquid and sealed using VALAP (vaseline:lanolin:paraffin, 1:1:1).

For the TEV-cleavage experiments, we used a modified protocol to maximize the number of bacteria lying flat on the coverslip; bacteria that are only partially attached to the coverslip often have regions that drift out of the focal plane and therefore cannot be used for analysis. For these experiments, 60 μl bacterial culture was placed on a poly-L-lysine-coated coverslip (22 mm; no. 1.5). After a 5 min incubation at room temperature, the coverslips were blotted and 50 μl of 3% glutaraldehyde were added to fix the bacteria to the coverslip. After 10 min, the coverslips were washed twice in PBS and immunofluorescence was performed using anti-ActA-PRR.

Microscopy. All imaging was performed on an upright Zeiss Axioplan 2 microscope equipped with a 100X Plan Apo objective lens (numerical aperture 1.4) and a 1,024×1,024-pixel back-illuminated EMCCD camera (Andor) using the MetaMorph software.

Image analysis. Morphometrics[55] was used to analyse images from the TEV-cleavage experiments. Briefly, segmentation of phase-contrast images was used to determine the cell outlines. Next, the mean fluorescence intensity for each cell was calculated as the total intensity within a cell outline minus the mean background fluorescence divided by the area of the cell. Normalization was performed by dividing the mean fluorescence intensity of a cell by the average intensity per cell for the untreated control population. Five independent TEV experiments were performed.

Electron microscopy. Bacterial strains were cultured for 16 h in the stated medium at 37 °C. Fixation and processing were performed using conventional procedures for TEM on bacterial samples. Briefly, approximately 2 ml of culture were spun down and fixed in 50 μl of 2% glutaraldehyde and 4% paraformaldehyde in 0.1 M sodium cacodylate buffer (pH 7.3) for 1 h at room temperature, followed by post-fixation in 1% osmium tetroxide for 1 h at 4 °C and then 1% uranyl acetate overnight. Dehydration using ethanol was followed by acetonitrile and finally embedding in Embed 812 (EMS, cat. no. 14120). Imaging of thin sections was performed on a JEOL1400 transmission electron microscope operating at 120 kV and 10,000× with a Gatan Orius 10.7 megapixel CCD camera. All of the steps from post-fixation to sectioning were conducted by staff at the Stanford Cell Sciences Imaging Facility. To measure wall thickness, images showing a section through the midplane of a bacterial cell were chosen and distances were quantified using ImageJ.

TEV cleavage. For each strain, 12 μl TEV buffer (1 M Tris–HCl pH 8 and 10 mM EDTA) and 2 μl of 100 mM DTT were added to 285 μl of growing culture. This mixture was aliquoted into two Eppendorf tubes (100 μl per tube) and 1 μl of purified TEV protease (1.1 mg ml^{-1}; purified from *E. coli* expressing His-tagged S219V TEV protease using plasmid pRK793 (Addgene)) was added to one of the tubes. The tubes were incubated at 30 °C for 45 min. The cells were then washed, and 60 μl were used for immunofluorescence and the remaining 40 μl were used for western blot analysis.

Western blotting. To extract ActA, bacteria were boiled in SDS–PAGE loading buffer, as previously described[14]. The bacterial cell wall was digested before sample preparation by adding *Listeria*-specific phage lysin Ply118 (ref. [56]). The primary antibody anti-ActA-PRR was used at a dilution of 1:10,000. Detection was performed using a chemiluminescent detection system using a horseradish peroxidase-conjugated goat anti-rabbit secondary antibody at 1:20,000 (SouthernBiotech)[7].

SDS–PAGE. SDS–PAGE was performed as previously described[57]. SDS-treated bacterial samples were diluted to 2.3 OD_{600} units ml^{-1} in sample buffer. For culture supernatants, bacterial culture equivalent to OD_{600} = 1 was clarified by centrifugation and the remaining proteins were concentrated to 150 μl in sample buffer by DOC/TCA precipitation as previously described[58].

Predicting disordered regions and surface proteins. Disordered regions for each protein from 294 prokaryotic species have previously been predicted[32] using the VSL2B predictor[33]. Proteins were categorized as surface proteins based on the presence of a predicted transmembrane domain (using TMHMM v2.0; ref. [59]),

signal sequence (using SignalP v3.0; ref. [60]) or a LPXTG motif[61,62]. Using these predictions, every disordered region of each protein was plotted as a cytosolic or surface protein (Fig. 6). The phylogenetic tree was generated using Interactive Tree Of Life[63]. In Table 1, surface proteins with disordered regions longer than 250 amino acids are listed for selected bacterial species.

Statistical analyses. The significance of differences between two distributions was computed using a two-sample Student's *t*-test.

Additional strain information. JAT817 (*PgsiB-actA*$^{1-639}$). *PgsiB*: *gsiB* promoter, activated in response to a variety of stresses. ActA$^{1-639}$: full-length *ActA* from *L. monocytogenes*.

JAT818 (PgsiB-iactA$^{1-1080}$*).* iActA$^{1-1080}$: full-length *iActA* from *L. ivanovii*.

JAT836 (tRNA^{Arg}*::PactA-actA*$^{1-30}$*-nup1*$^{220-797}$*-actA*$^{600-639}$*). PactA*: *actA* promoter. *ActA*$^{1-30}$: signal sequence of ActA. Nup1$^{220-797}$: previously characterized disordered region of the Nup1 nuclear pore protein[23]. ActA$^{600-639}$: transmembrane region of ActA, which includes a short cytosolic tail of a few amino acids. This construct has a C-terminal transmembrane domain.

JAT840 (tRNA^{Arg}*::PactA-actA*$^{1-30}$*-nsp1*$^{173-603}$*-actA*$^{600-639}$*).* Nsp1$^{173-603}$: previously characterized disordered region of the Nsp1 nuclear pore protein[23]. This construct has a C-terminal transmembrane domain.

JAT889 (tRNA^{Arg}*::PactA-lmo2229*$^{1-61}$*-nsp1*$^{7-603}$*).* lmo2229$^{1-61}$: transmembrane region of lmo2229, which includes a cytosolic tail of around 40 amino acids. Nsp1$^{7-603}$: disordered region of the Nsp1 nuclear pore protein. This construct has an N-terminal transmembrane domain.

JAT890 (tRNA^{Arg}*::PactA-lmo2039*$^{1-31}$*-nsp1*$^{7-603}$*).* lmo2039$^{1-31:}$ transmembrane region of lmo2039, which includes a cytosolic tail of around ten amino acids. This construct has an N-terminal transmembrane domain.

JAT915 (tRNA^{Arg}*::PactA-actA*$^{1-30}$*-nsp1*$^{7-603}$*).* Nsp1$^{7-603}$ with an N-terminal signal sequence (ActA$^{1-30}$) but no transmembrane domain.

JAT1006 (tRNA^{Arg}*::PactA-lmo2229*$^{1-61}$*-nsp1*$^{7-603}$*-actA*$^{600-639}$*).* Nsp1$^{7-603}$ with N-terminal (lmo2229$^{1-61}$) and C-terminal (ActA$^{600-639}$) transmembrane domains.

JAT1024 (comK::PactA-actA$^{1-6}$*-TEV-actA*$^{64-639}$*).* ActA with TEV sequence placed between amino acids 63 and 64 (relative to the start codon).

JAT1025 (comK::PactA-actA$^{1-139}$*-TEV-actA*$^{140-639}$*).* ActA with TEV sequence placed between amino acids 139 and 140.

JAT1026 (comK::PactA-actA$^{1-164}$*-TEV-ActA*$^{165-639}$*).* ActA with TEV sequence placed between amino acids 164 and 165.

JAT1027 (comK::PactA-actA$^{1-196}$*-TEV-ActA*$^{197-639}$*).* ActA with the TEV sequence placed between amino acids 196 and 197.

JAT1028 (comK::PactA-actA$^{1-210}$*-TEV-actA*$^{211-639}$*).* ActA with TEV sequence placed between amino acids 210 and 211.

JAT1024–1028. The TEV protease recognition sequence (ENLYFQG) was inserted into ActA where designated. Here, the position of the TEV recognition sequence within ActA is relative to the start codon. In the manuscript, these constructs are labelled as TEV-33, TEV-109, TEV-134, TEV-166, and TEV-180. These numbers correspond to the number of amino acids after the signal peptidase cleavage site and not the number of amino acids after the start codon.

JAT1037 (Pspa-spa$^{1-51}$*-nsp*$^{173-603}$*-actA*$^{600-639}$*). Pspa*: protein A (*spa*) promoter. SpA$^{1-51}$: protein A (SpA) signal sequence.

JAT1040 (tRNA^{Arg}*::Pspac/lacOid-actA*$^{1-639}$*). Pspac/lacOid*: SPAC/lacOid IPTG-inducible promoter.

For strains JAT817 and JAT818, constructs were inserted into the previously described non-integrating, expression vector pHCMC03 (ref. [52]). For strain JAT1037, the non-integrating vector pOS1 was used[54]. The remaining strains used the integrating vectors pPL1 or pPL2 (ref. [53]), as described in the 'Strain construction' section.

Reporting Summary. Further information on research design is available in the Nature Research Reporting Summary linked to this article.

Data availability

All data are available upon request from the corresponding authors. Source data are provided with this paper.

Code availability

All custom scripts are available at https://bitbucket.org/kchuanglab/acta_code/src/master/.

Received: 17 December 2020; Accepted: 28 June 2021;
Published online: 29 July 2021

References

1. Finlay, B. B. & Falkow, S. Common themes in microbial pathogenicity revisited. *Microbiol. Mol. Biol. Rev.* **61**, 136–169 (1997).
2. Pizarro-Cerda, J. & Cossart, P. Bacterial adhesion and entry into host cells. *Cell* **124**, 715–727 (2006).
3. Demchick, P. & Koch, A. L. The permeability of the wall fabric of *Escherichia coli* and *Bacillus subtilis*. *J. Bacteriol.* **178**, 768–773 (1996).
4. Forster, B. M. & Marquis, H. Protein transport across the cell wall of monoderm Gram-positive bacteria. *Mol. Microbiol.* **84**, 405–413 (2012).
5. Schneewind, O. & Missiakas, D. M. Protein secretion and surface display in Gram-positive bacteria. *Philos. Trans. R. Soc. B* **367**, 1123–1139 (2012).
6. Matias, V. R. & Beveridge, T. J. Cryo-electron microscopy reveals native polymeric cell wall structure in *Bacillus subtilis* 168 and the existence of a periplasmic space. *Mol. Microbiol.* **56**, 240–251 (2005).
7. Rafelski, S. M. & Theriot, J. A. Mechanism of polarization of *Listeria monocytogenes* surface protein ActA. *Mol. Microbiol.* **59**, 1262–1279 (2006).
8. Welch, M. D., Rosenblatt, J., Skoble, J., Portnoy, D. A. & Mitchison, T. J. Interaction of human Arp2/3 complex and the *Listeria monocytogenes* ActA protein in actin filament nucleation. *Science* **281**, 105–108 (1998).
9. Kocks, C. et al. *L. monocytogenes*-induced actin assembly requires the actA gene product, a surface protein. *Cell* **68**, 521–531 (1992).
10. Tilney, L. G. & Portnoy, D. A. Actin filaments and the growth, movement, and spread of the intracellular bacterial parasite, *Listeria monocytogenes*. *J. Cell Biol.* **109**, 1597–1608 (1989).
11. Kocks, C. et al. The unrelated surface proteins ActA of *Listeria monocytogenes* and IcsA of *Shigella flexneri* are sufficient to confer actin-based motility on *Listeria innocua* and *Escherichia coli* respectively. *Mol. Microbiol.* **18**, 413–423 (1995).
12. Smith, G. A., Portnoy, D. A. & Theriot, J. A. Asymmetric distribution of the *Listeria monocytogenes* ActA protein is required and sufficient to direct actin-based motility. *Mol. Microbiol.* **17**, 945–951 (1995).
13. Beckerle, M. C. Spatial control of actin filament assembly: lessons from *Listeria*. *Cell* **95**, 741–748 (1998).
14. Footer, M. J., Lyo, J. K. & Theriot, J. A. Close packing of *Listeria monocytogenes* ActA, a natively unfolded protein, enhances F-actin assembly without dimerization. *J. Biol. Chem.* **283**, 23852–23862 (2008).
15. Housden, N. G. et al. Intrinsically disordered protein threads through the bacterial outer-membrane porin OmpF. *Science* **340**, 1570–1574 (2013).
16. Driessen, A. J. & Nouwen, N. Protein translocation across the bacterial cytoplasmic membrane. *Annu. Rev. Biochem.* **77**, 643–667 (2008).
17. Silhavy, T. J., Kahne, D. & Walker, S. The bacterial cell envelope. *Cold Spring Harb. Perspect. Biol.* **2**, a000414 (2010).
18. Dubrac, S., Bisicchia, P., Devine, K. M. & Msadek, T. A matter of life and death: cell wall homeostasis and the WalKR (YycGF) essential signal transduction pathway. *Mol. Microbiol.* **70**, 1307–1322 (2008).
19. Devine, K. M. Bacterial L-forms on tap: an improved methodology to generate *Bacillus subtilis* L-forms heralds a new era of research. *Mol. Microbiol.* **83**, 10–13 (2012).
20. Wu, X. C., Lee, W., Tran, L. & Wong, S. L. Engineering a *Bacillus subtilis* expression-secretion system with a strain deficient in six extracellular proteases. *J. Bacteriol.* **173**, 4952–4958 (1991).
21. Zuber, B. et al. Granular layer in the periplasmic space of Gram-positive bacteria and fine structures of *Enterococcus gallinarum* and *Streptococcus gordonii* septa revealed by cryo-electron microscopy of vitreous sections. *J. Bacteriol.* **188**, 6652–6660 (2006).
22. Gouin, E., Dehoux, P., Mengaud, J., Kocks, C. & Cossart, P. iactA of *Listeria ivanovii*, although distantly related to *Listeria monocytogenes* actA, restores actin tail formation in an *L. monocytogenes* actA mutant. *Infect. Immun.* **63**, 2729–2737 (1995).
23. Kreft, J., Dumbsky, M. & Theiss, S. The actin-polymerization protein from *Listeria ivanovii* is a large repeat protein which shows only limited amino acid sequence homology to ActA from *Listeria monocytogenes*. *FEMS Microbiol. Lett.* **132**, 181–182 (1995).
24. Yamada, J. et al. A bimodal distribution of two distinct categories of intrinsically disordered structures with separate functions in FG nucleoporins. *Mol. Cell Proteom.* **9**, 2205–2224 (2010).
25. Matias, V. R. & Beveridge, T. J. Native cell wall organization shown by cryo-electron microscopy confirms the existence of a periplasmic space in *Staphylococcus aureus*. *J. Bacteriol.* **188**, 1011–1021 (2006).
26. DeDent, A. C., McAdow, M. & Schneewind, O. Distribution of protein A on the surface of *Staphylococcus aureus*. *J. Bacteriol.* **189**, 4473–4484 (2007).

27. DeDent, A., Bae, T., Missiakas, D. M. & Schneewind, O. Signal peptides direct surface proteins to two distinct envelope locations of *Staphylococcus aureus*. *EMBO J.* **27**, 2656–2668 (2008).
28. Alonzo, F. 3rd & Freitag, N. E. *Listeria monocytogenes* PrsA2 is required for virulence factor secretion and bacterial viability within the host cell cytosol. *Infect. Immun.* **78**, 4944–4957 (2010).
29. Bauer, B. W., Shemesh, T., Chen, Y. & Rapoport, T. A. A "push and slide" mechanism allows sequence-insensitive translocation of secretory proteins by the SecA ATPase. *Cell* **157**, 1416–1429 (2014).
30. Downer, R., Roche, F., Park, P. W., Mecham, R. P. & Foster, T. J. The elastin-binding protein of *Staphylococcus aureus* (EbpS) is expressed at the cell surface as an integral membrane protein and not as a cell wall-associated protein. *J. Biol. Chem.* **277**, 243–250 (2002).
31. Okuda, S., Freinkman, E. & Kahne, D. Cytoplasmic ATP hydrolysis powers transport of lipopolysaccharide across the periplasm in *E. coli*. *Science* **338**, 1214–1217 (2012).
32. Pavlovic-Lazetic, G. M. et al. Bioinformatics analysis of disordered proteins in prokaryotes. *BMC Bioinform.* **12**, 66 (2011).
33. Peng, K., Radivojac, P., Vucetic, S., Dunker, A. K. & Obradovic, Z. Length-dependent prediction of protein intrinsic disorder. *BMC Bioinform.* **7**, 208 (2006).
34. Cacciuto, A. & Luijten, E. Confinement-driven translocation of a flexible polymer. *Phys. Rev. Lett.* **96**, 238104 (2006).
35. Gopinathan, A. & Kim, Y. W. Polymer translocation in crowded environments. *Phys. Rev. Lett.* **99**, 228106 (2007).
36. Luo, K., Metzler, R., Ala-Nissila, T. & Ying, S. C. Polymer translocation out of confined environments. *Phys. Rev. E* **80**, 021907 (2009).
37. Muthukumar, M. Translocation of a confined polymer through a hole. *Phys. Rev. Lett.* **86**, 3188–3191 (2001).
38. Muthukumar, M. Molecular modelling of nucleation in polymers. *Philos. Trans. A* **361**, 539–556 (2003).
39. Park, P. J. & Sung, W. Polymer release out of a spherical vesicle through a pore. *Phys. Rev. E* **57**, 730 (1998).
40. Rubinstein, M. & Colby, R. H. *Polymer Physics* Vol. 23 (Oxford Univ. Press, 2003).
41. Sung, W. & Park, P. J. Polymer translocation through a pore in a membrane. *Phys. Rev. Lett.* **77**, 783–786 (1996).
42. Edwards, M. R. & Stevens, R. W. Fine structure of *Listeria monocytogenes*. *J. Bacteriol.* **86**, 414–428 (1963).
43. North, R. J. Some structural aspects of *Listeria Monocytogenes*. *J. Ultrastruct. Res.* **59**, 187–197 (1963).
44. De Gennes, P.-G. & Gennes, P.-G. *Scaling Concepts in Polymer Physics* (Cornell Univ. Press, 1979).
45. Clisby, N. & Dunweg, B. High-precision estimate of the hydrodynamic radius for self-avoiding walks. *Phys. Rev. E* **94**, 052102 (2016).
46. Flory, P. *Principles of Polymer Chemistry* (Cornell Univ. Press, 1971).
47. Grundling, A., Gonzalez, M. D. & Higgins, D. E. Requirement of the *Listeria monocytogenes* broad-range phospholipase PC-PLC during infection of human epithelial cells. *J. Bacteriol.* **185**, 6295–6307 (2003).
48. Shen, A., Kamp, H. D., Grundling, A. & Higgins, D. E. A bifunctional O-GlcNAc transferase governs flagellar motility through anti-repression. *Genes Dev.* **20**, 3283–3295 (2006).
49. Ripio, M. T., Brehm, K., Lara, M., Suarez, M. & Vazquez-Boland, J. A. Glucose-1-phosphate utilization by *Listeria monocytogenes* is PrfA dependent and coordinately expressed with virulence factors. *J. Bacteriol.* **179**, 7174–7180 (1997).
50. Ripio, M. T. et al. Transcriptional activation of virulence genes in wild-type strains of *Listeria monocytogenes* in response to a change in the extracellular medium composition. *Res. Microbiol.* **147**, 371–384 (1996).
51. Maul, B., Volker, U., Riethdorf, S., Engelmann, S. & Hecker, M. σ^B-Dependent regulation of *gsiB* in response to multiple stimuli in *Bacillus subtilis*. *Mol. Gen. Genet.* **248**, 114–120 (1995).
52. Nguyen, H. D. et al. Construction of plasmid-based expression vectors for *Bacillus subtilis* exhibiting full structural stability. *Plasmid* **54**, 241–248 (2005).
53. Lauer, P., Chow, M. Y., Loessner, M. J., Portnoy, D. A. & Calendar, R. Construction, characterization, and use of two *Listeria monocytogenes* site-specific phage integration vectors. *J. Bacteriol.* **184**, 4177–4186 (2002).
54. Schneewind, O., Mihaylova-Petkov, D. & Model, P. Cell wall sorting signals in surface proteins of Gram-positive bacteria. *EMBO J.* **12**, 4803–4811 (1993).
55. Ursell, T. et al. Rapid, precise quantification of bacterial cellular dimensions across a genomic-scale knockout library. *BMC Biol.* **15**, 17 (2017).
56. Loessner, M. J., Kramer, K., Ebel, F. & Scherer, S. C-terminal domains of *Listeria monocytogenes* bacteriophage murein hydrolases determine specific recognition and high-affinity binding to bacterial cell wall carbohydrates. *Mol. Microbiol.* **44**, 335–349 (2002).
57. Laemmli, U. K. Cleavage of structural proteins during the assembly of the head of bacteriophage T4. *Nature* **227**, 680–685 (1970).
58. Koontz, L. TCA precipitation. *Methods Enzymol.* **541**, 3–10 (2014).
59. Krogh, A., Larsson, B., von Heijne, G. & Sonnhammer, E. L. Predicting transmembrane protein topology with a hidden Markov model: application to complete genomes. *J. Mol. Biol.* **305**, 567–580 (2001).
60. Bendtsen, J. D., Nielsen, H., von Heijne, G. & Brunak, S. Improved prediction of signal peptides: SignalP 3.0. *J. Mol. Biol.* **340**, 783–795 (2004).
61. Fischetti, V. A., Pancholi, V. & Schneewind, O. Conservation of a hexapeptide sequence in the anchor region of surface proteins from Gram-positive cocci. *Mol. Microbiol.* **4**, 1603–1605 (1990).
62. Schneewind, O., Model, P. & Fischetti, V. A. Sorting of protein A to the staphylococcal cell wall. *Cell* **70**, 267–281 (1992).
63. Letunic, I. & Bork, P. Interactive Tree Of Life (iTOL): an online tool for phylogenetic tree display and annotation. *Bioinformatics* **23**, 127–128 (2007).

Acknowledgements

We thank M. Rexach for the antibody against Nsp1; W. Burkholder, A. Cheung, T. Burke, and D. Portnoy for strains; and J. Lynch, K. Schulz, H. Shi, M. Tsuchida, and S. Weber for comments on the manuscript. Electron microscopy was performed at, and with the assistance of, the Stanford Cell Sciences Imaging Facility. This work was supported by the National Institutes of Health (NIH) grant no. R37AI-36929 (to J.A.T.); an NSF CAREER Award (grant no. MCB-1149328 to K.C.H.); NSF grant nos. DBI-0960480, DMS-1616926, and HRD-1547848 (to A.G.), and EF-1038697 (to A.G. and K.C.H.); a James S. McDonnell Foundation Award (to A.G.); the Allen Center for Systems Modeling of Infection (to K.M.N. and K.C.H.) and HHMI (to J.A.T.). The project was supported, in part, by an ARRA Award (grant no. 1S10RR026780-01) from the National Center for Research Resources (NCRR); its contents are solely the responsibility of the authors and do not necessarily represent the official views of the NCRR or the NIH. K.C.H. is a Chan Zuckerberg Biohub Investigator.

Author contributions

D.K.H., F.E.O., K.C.H. and J.A.T. designed the experiments, analysed the data and wrote the manuscript. D.K.H., F.E.O., M.J.F. and J.A.T. performed the experiments. D.K.H. and K.M.N. constructed the mutants. A.G. and K.C.H. developed the model. N.S.M. and S.N.M. performed the disorder predictions. All authors reviewed the manuscript before submission.

Competing interests

The authors declare no competing interests.

Additional information

Extended data is available for this paper at https://doi.org/10.1038/s41564-021-00942-8.

Supplementary information The online version contains supplementary material available at https://doi.org/10.1038/s41564-021-00942-8.

Correspondence and requests for materials should be addressed to K.C.H. or J.A.T.

Peer review information *Nature Microbiology* thanks the anonymous reviewers for their contribution to the peer review of this work.

Reprints and permissions information is available at www.nature.com/reprints.

Publisher's note Springer Nature remains neutral with regard to jurisdictional claims in published maps and institutional affiliations.

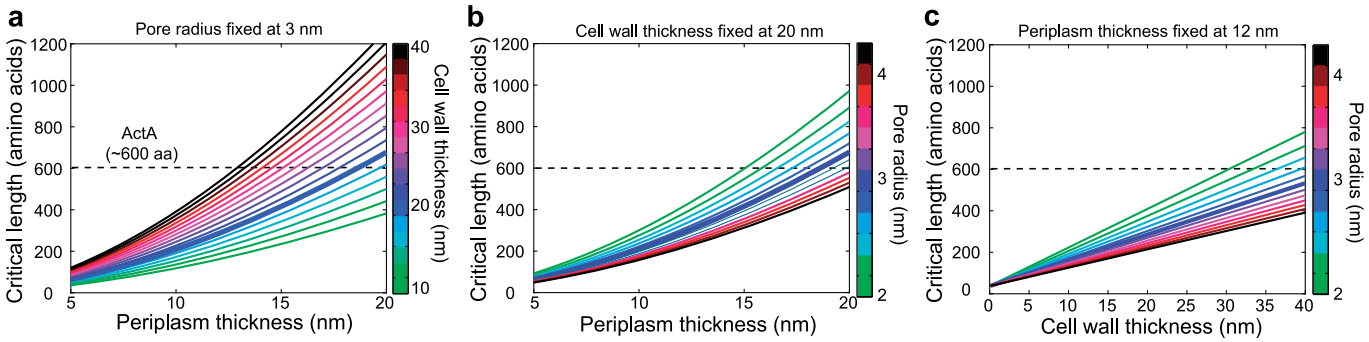

Extended Data Fig. 1 | Predicted critical lengths for an ActA-like polymer for different values of cell wall thickness, periplasm thickness and pore radius. a) Critical length as a function of periplasm thickness P for different values of cell wall thickness w, with pore radius R set at 3 nm. Each curve denotes a different cell wall thickness, with w ranging from 10 nm to 40 nm. b) Critical length as a function of periplasm thickness P for different values of R, with w set at 20 nm. c) Critical length as a function of cell wall thickness w for different values of R, with P set at 12 nm. In (**b**,**c**), each curve denotes a different pore radius, with R ranging from 2 nm to 4.2 nm. For all graphs the thickest line signifies parameters used in Fig. 1: $w = 20$ nm, $P = 12$ nm, $R = 3$ nm. The dashed horizontal line denotes the length of an ActA molecule. The entropic model predicts that any parameter set resulting in a critical length falling below this dashed line will result in proper translocation of ActA. All parameter values were chosen so that $2R$ and P are substantially more than the persistence length of ActA.

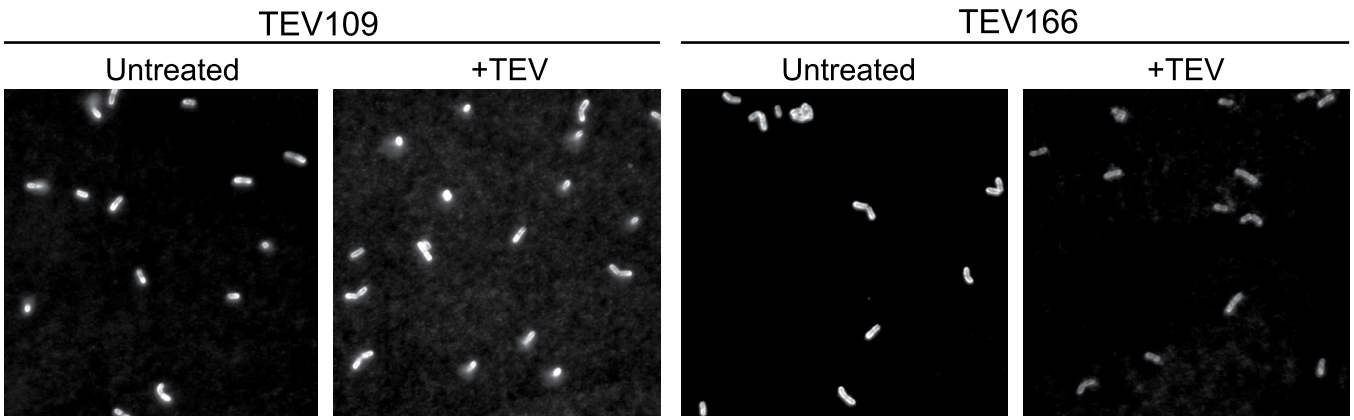

Extended Data Fig. 2 | Effects of TEV protease treatment on surface presentation of ActA. A representative TEV cleavage experiment showing population distributions of untreated and TEV protease-treated conditions for strains in Fig. 2d,e after labelling with α–ActA-PRR.

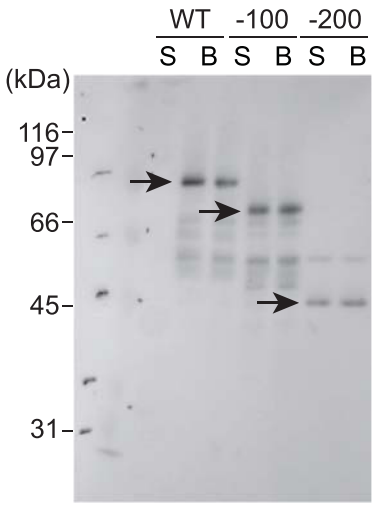

Extended Data Fig. 3 | Genetic truncations of ActA were detected at expected lengths. -100 and -200 refer to 100- and 200-amino acid truncation mutants, respectively. SDS treatment (S) and mechanical disruption by bead-beating (B) as in Fig. 1a,b were performed for all strains labelled with α–ActA-PRR. Arrows indicate (from left to right) full-length ActA, the 100-amino acid truncation, and the 200-amino acid truncation.

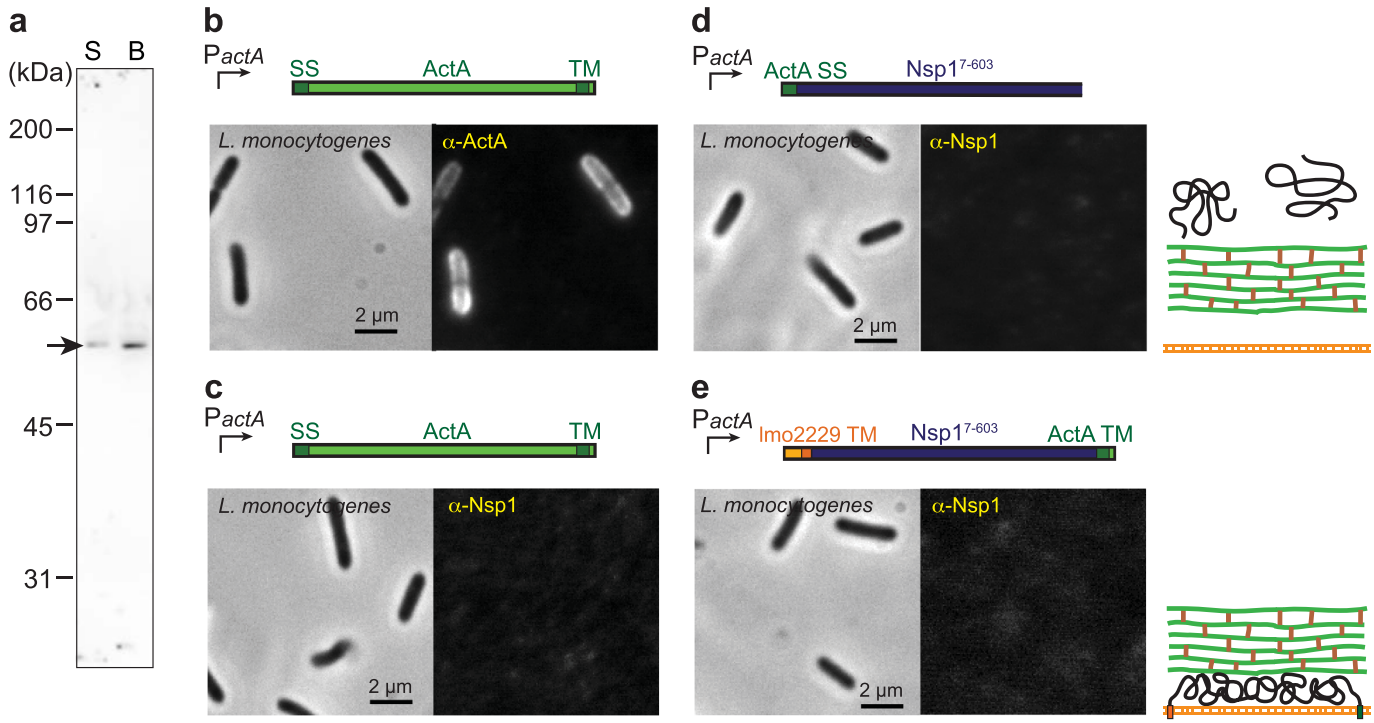

Extended Data Fig. 4 | Lack of immunofluorescence signal for Nsp1 constructs that are secreted or anchored by transmembrane domains at both termini. a) Western blotting showed stable expression of the Nsp1 chimaeric construct (arrow) from Fig. 5a,b. b) Polar distribution of ActA in the wild-type strain of *L. monocytogenes* using an antibody against ActA. c) Lack of signal in the wild-type strain using an antibody against Nsp1. d) Immunofluorescence of Nsp1 expressed with an amino-terminal signal sequence from ActA but no transmembrane anchor. e) Nsp1 expressed with an amino-terminal transmembrane domain from lmo2229 and carboxy-terminal5 transmembrane domain from ActA. No visible labelling was observed when Nsp1 was anchored at both ends, confirming that antibodies do not label proteins that are trapped in the periplasm.

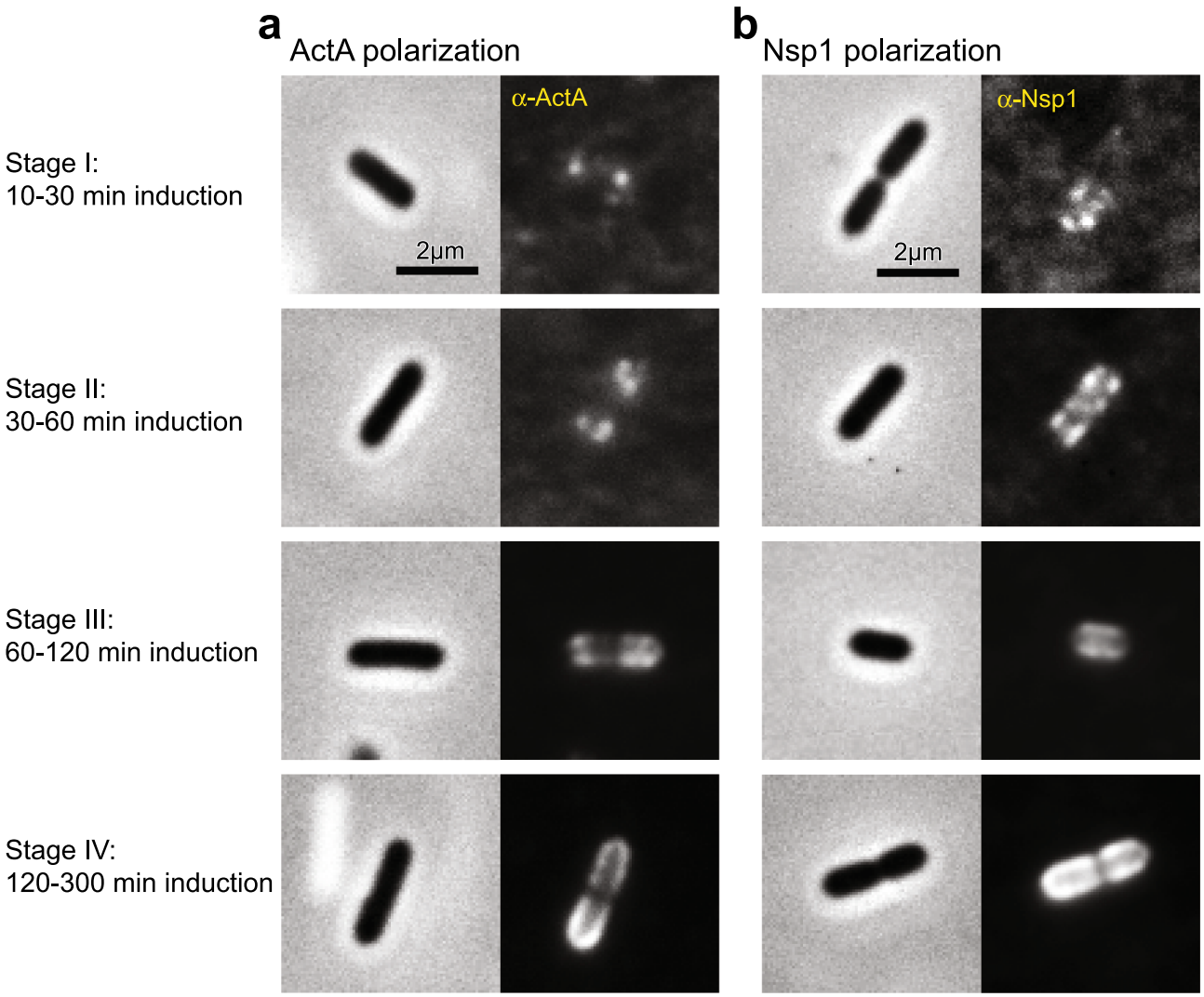

Extended Data Fig. 5 | Time course of disordered protein localization and polarization in *L. monocytogenes*. a) ActA expressed from the ActA promoter. b) Nsp1, with a signal sequence and transmembrane domain from ActA, expressed from the ActA promoter.

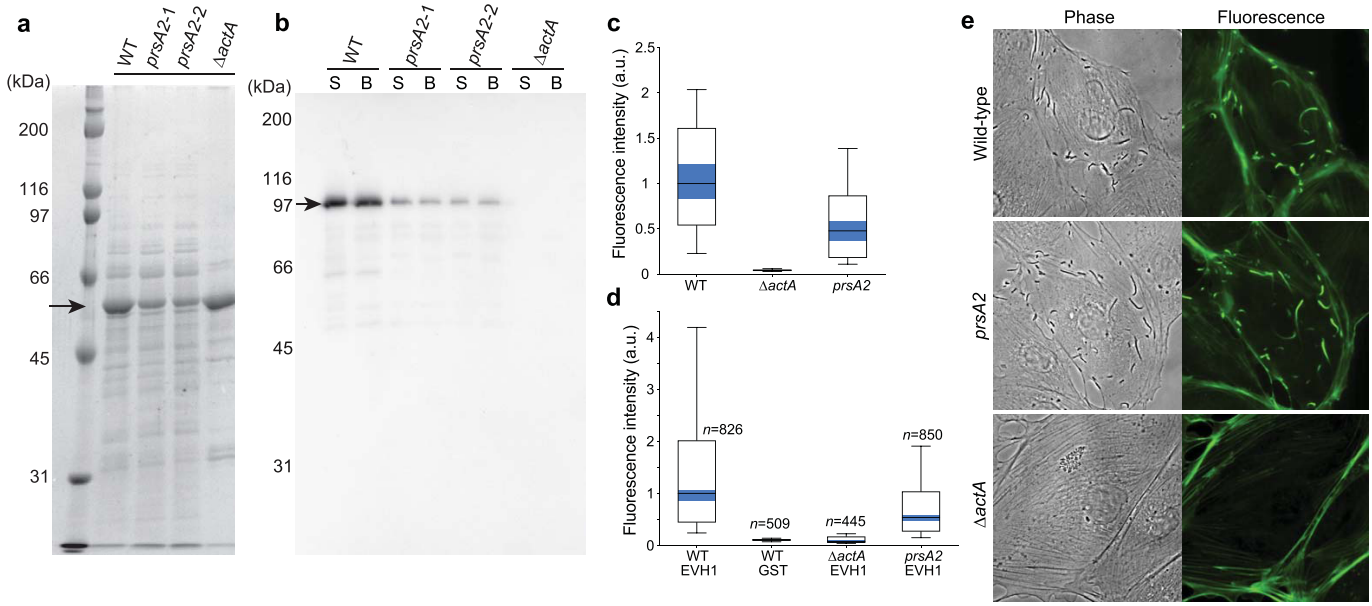

Extended Data Fig. 6 | ActA expression, translocation, and exposure, as well as VASP binding and comet-tail formation, were maintained in Δ*prsA2* cells. a) Expression of listeriolysin O (arrow) was lower in two *prsA2* transposon insertion mutants, as expected, but similar to wild type in a Δ*actA* mutant, as shown in a Coomassie-stained gel of TCA-precipitated culture supernatant. b) Expression of ActA (arrow) in *prsA2* cells determined using α−ActA decreased to a similar extent as listeriolysin O in (**a**); no expression was detected in Δ*actA* cells. Levels were similar between cells treated with SDS (S) or subjected to bead-beating (B), indicating that most ActA was translocated across the cell wall. c) Immunofluorescence labelling with α−ActA confirmed that ActA was exposed on the surface of wild-type and *prsA2* cells. d) The EVH1 domain of VASP fused to GST bound to the surface of *prsA2* and wild-type cells expressing wild-type ActA, but not to a Δ*actA* cells. GST alone also did not bind the surface of wild-type bacteria. Shown is immunofluorescence labelling of GST. e) Wild-type and *prsA2 L. monocytogenes* formed comet tails in host cells, but Δ*actA L. monocytogenes* did not. Actin was labelled with phalloidin. Thus, PrsA2 is not required for ActA translocation or function.

nature research

Corresponding author(s): Kerwyn Casey Huang

Last updated by author(s): 11/19/2020

Reporting Summary

Nature Research wishes to improve the reproducibility of the work that we publish. This form provides structure for consistency and transparency in reporting. For further information on Nature Research policies, see Authors & Referees and the Editorial Policy Checklist.

Statistics

For all statistical analyses, confirm that the following items are present in the figure legend, table legend, main text, or Methods section.

n/a	Confirmed
☐	☒ The exact sample size (*n*) for each experimental group/condition, given as a discrete number and unit of measurement
☐	☒ A statement on whether measurements were taken from distinct samples or whether the same sample was measured repeatedly
☐	☒ The statistical test(s) used AND whether they are one- or two-sided *Only common tests should be described solely by name; describe more complex techniques in the Methods section.*
☒	☐ A description of all covariates tested
☒	☐ A description of any assumptions or corrections, such as tests of normality and adjustment for multiple comparisons
☐	☒ A full description of the statistical parameters including central tendency (e.g. means) or other basic estimates (e.g. regression coefficient) AND variation (e.g. standard deviation) or associated estimates of uncertainty (e.g. confidence intervals)
☐	☒ For null hypothesis testing, the test statistic (e.g. *F*, *t*, *r*) with confidence intervals, effect sizes, degrees of freedom and *P* value noted *Give P values as exact values whenever suitable.*
☒	☐ For Bayesian analysis, information on the choice of priors and Markov chain Monte Carlo settings
☒	☐ For hierarchical and complex designs, identification of the appropriate level for tests and full reporting of outcomes
☒	☐ Estimates of effect sizes (e.g. Cohen's *d*, Pearson's *r*), indicating how they were calculated

Our web collection on statistics for biologists contains articles on many of the points above.

Software and code

Policy information about availability of computer code

Data collection	Microscopy data were acquired using Metamorph.
Data analysis	Data analyses were performed using MATLAB. For single-cell analyses, the software package Morphometrics v. 1.1 was used.

For manuscripts utilizing custom algorithms or software that are central to the research but not yet described in published literature, software must be made available to editors/reviewers. We strongly encourage code deposition in a community repository (e.g. GitHub). See the Nature Research guidelines for submitting code & software for further information.

Data

Policy information about availability of data

All manuscripts must include a data availability statement. This statement should provide the following information, where applicable:

- Accession codes, unique identifiers, or web links for publicly available datasets
- A list of figures that have associated raw data
- A description of any restrictions on data availability

The datasets generated during and/or analysed during the current study are available from the corresponding authors on reasonable request.

Field-specific reporting

Please select the one below that is the best fit for your research. If you are not sure, read the appropriate sections before making your selection.

☒ Life sciences ☐ Behavioural & social sciences ☐ Ecological, evolutionary & environmental sciences

For a reference copy of the document with all sections, see nature.com/documents/nr-reporting-summary-flat.pdf

Life sciences study design

All studies must disclose on these points even when the disclosure is negative.

Sample size	No sample-size calculation was performed.
Data exclusions	No data were excluded from the analyses.
Replication	All attempts at replication were successful.
Randomization	Randomization was not relevant to this study.
Blinding	Blinding was not relevant to this study.

Reporting for specific materials, systems and methods

We require information from authors about some types of materials, experimental systems and methods used in many studies. Here, indicate whether each material, system or method listed is relevant to your study. If you are not sure if a list item applies to your research, read the appropriate section before selecting a response.

Materials & experimental systems

n/a	Involved in the study
☐	☒ Antibodies
☒	☐ Eukaryotic cell lines
☒	☐ Palaeontology
☒	☐ Animals and other organisms
☒	☐ Human research participants
☒	☐ Clinical data

Methods

n/a	Involved in the study
☒	☐ ChIP-seq
☒	☐ Flow cytometry
☒	☐ MRI-based neuroimaging

Antibodies

Antibodies used	Antibodies used: rabbit polyclonal anti-peptide antibody against the first proline-rich repeat of ActA; rabbit polyclonal antibody against full length ActA; rabbit polyclonal antibody against the FG-region of Nsp1 (generous gift from Michael Rexach, University of California at Santa Cruz) or Abcam anti-Nsp1 antibody 32D6; Alexa Fluor-488 goat anti-rabbit antibody (Invitrogen).
Validation	ActA antibodies were validated in Rafelski and Theriot, Molecular Microbiology 59 1262-1279 (2006). Abcam anti-Nsp1 antibody validation can be found at https://www.abcam.com/nsp1-antibody-32d6-ab4641.html?productWallTab=ShowAll.